Hypervelocity Impact Performance of Open Cell Foam Core Sandwich Panel Structures

S. Ryan[*,1], E. Ordonez[2], E. L. Christiansen[3], D. M. Lear[3]
[1]*USRA Lunar and Planetary Institute, 3600 Bay Area Blvd, Houston, TX, 77058, USA*
[2]*MEI Technologies Inc/ESCG, 2224 Bay Area Blvd, Houston, TX, 77058, USA*
[3]*NASA Johnson Space Center, 2101 NASA Pkwy, Houston, TX, 77058, USA*

Received Date Line (to be inserted by Production) (8 pt)

Abstract

Open cell metallic foam core sandwich panel structures are of interest for application in spacecraft micrometeoroid and orbital debris shields due to their novel form and advantageous structural and thermal performance. Repeated shocking as a result of secondary impacts upon individual foam ligaments during the penetration process acts to raise the thermal state of impacting projectiles, resulting in fragmentation, melting, and vaporization at lower velocities than with traditional shielding configurations (e.g. Whipple shield). In order to characterize the protective capability of these structures, an extensive experimental campaign was performed by the Johnson Space Center Hypervelocity Impact Technology Facility, the results of which are reported in this paper. Although not capable of competing against the protection levels achievable with leading heavy shields in use on modern high-risk vehicles (i.e. International Space Station modules), metallic foam core sandwich panels are shown to provide a substantial improvement over comparable structural panels and traditional low weight shielding alternatives such as honeycomb sandwich panels and metallic Whipple shields. A ballistic limit equation, generalized in terms of panel geometry, is derived and presented in a form suitable for application in risk assessment codes.

Keywords: Hypervelocity impact, orbital debris, space environment, cellular materials

*Corresponding author. Tel.: +1 281 413-2983; fax: +1 281 483-3908.
E-mail address: shannon.j.ryan@nasa.gov

1. Introduction

Mission restrictions (e.g. weight, launch volume, etc.) often prevent the inclusion of a dedicated protective structure for space vehicles against micrometeoroid and orbital debris (MMOD) impact. In such cases, the vehicle primary structure acts as the de facto shield. As a result, honeycomb sandwich panels with aluminum or composite facesheets are amongst the most common MMOD shields, despite being unsuited to this task. For impacts in which generated pressures are sufficient to induce projectile fragmentation, the presence of the honeycomb cell walls acts to limit the expansion of the debris cloud as it propagates through the thickness of the panel core, a phenomenon commonly referred to as channeling (e.g. [1]). Although honeycomb cell foils are not sufficiently thick to prevent penetration by individual fragments, particles impacting at shallow angles of incidence ricochet from the cell walls, effectively concentrating a substantial percentage of the debris cloud within a confined area. For aluminum on aluminum impacts, a ricochet angle of 60-65° is commonly defined (e.g. [2]).

Metallic foams are a relatively new class of materials with low density and novel physical, mechanical, thermal, electrical and acoustic properties. Although incompletely characterized, they offer comparable mechanical performance to traditional spacecraft primary structures without features detrimental to MMOD shielding (i.e. through-thickness channeling cells). There are two competing types of metallic foams: open cell and closed cell. Open cell foams are considered the more promising technology due to their lower weight and higher degree of homogeneity.

The performance of metallic open cell foam core sandwich panels has been the subject of a recent investigation at NASA Johnson Space Center's Hypervelocity Impact Technology Facility (HITF). In this paper, the results of this experimental program are reported, and the applicability of metallic foam core sandwich panel structures to MMOD shielding is evaluated.

2. Description of the investigated material

In this study, Duocel© open cell aluminum foams from ERG Aerospace have been selected for testing. Duocel foams are manufactured through utilization of a solid negative-image ceramic mould, which is filled with a liquid aluminum alloy and allowed to cool. The individual cells are typically 14-faceted polyhedral or solid tetrakaidecahedrons. Once the foam has solidified, the thin membranes or windows are removed through a reticulation process, leaving behind only interconnected struts which form the open-cell structure. The tetrakaidecahedrons are referred to as cells, and the individual windows between the interconnected foam ligaments are the pores, shown in Fig. 1. The pore size controls the number and nominal size of foam ligaments, while the foam relative density controls their cross-sectional form and actual size. Examples of ligament cross-sections are also provided in Fig. 1.

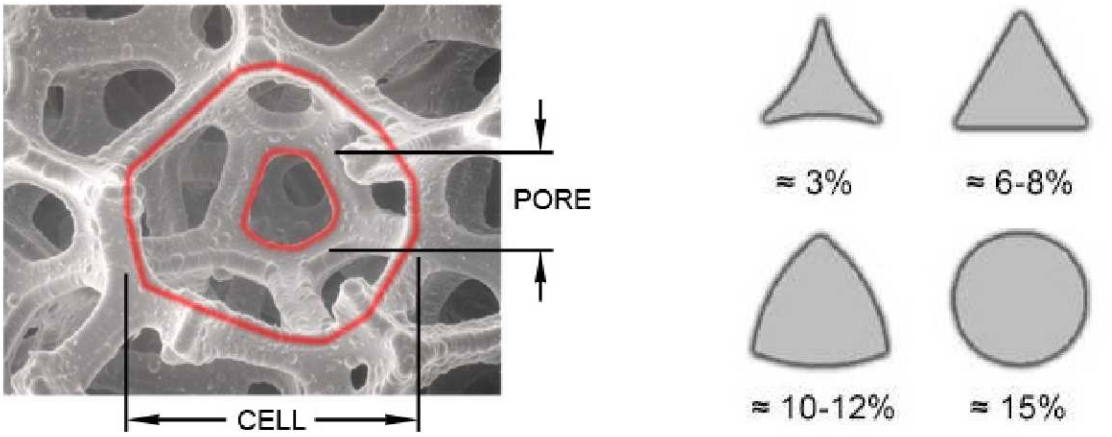

Fig. 1. Open cell foam pore and cell size (left), and ligament cross section variation with relative density (© ERG Aerospace)

3. Impact Testing

A total of 81 hypervelocity impact tests have been performed on open cell foam core sandwich panels over a range of impact angles (0°/45°/60°) and velocities (2.18-7.56 km/s). The performance has been evaluated for panels with varying pore densities (10/20/40 PPI), core (12.7/25.4/50.8 mm) and

facesheet (0.254/0.381/0.508 mm) thicknesses. All impact tests have been performed at the NASA Johnson Space Center White Sands Test Facility (WSTF), on the 0.17- and 0.50-cal two stage light gas gun ranges. In all experiments a 1.016 mm thick Al2024-T3 witness plate was located 100 mm from the sandwich panel rear side, held in place via threaded rods, the front side of which was dusted with a thin coat of blue paint to enhance the visibility of ejecta deposits. The experimental setup is shown in Fig. 2.

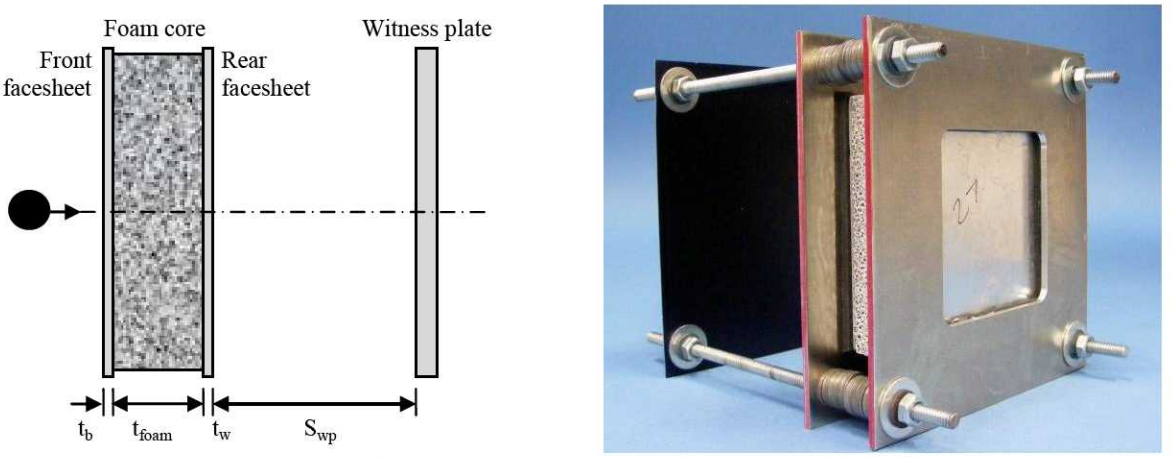

Fig. 2. Schematic (left) and pre-test photograph (right) of the experimental setup

A summary of test conditions and results is given in Table 1. In these tests, failure was defined as the onset of material ejection from the sandwich panel rear facesheet (i.e. detached spall). The test results are defined as significantly above (>>), above (>), minimally above (≥), equal to (=), minimally below (≤), below (<), and significantly below (<<) the failure threshold. For example, an impact test which results in no visible damage to the panel rear facesheet (i.e. no deformation or bulging) is considered significantly below the failure threshold (<<). A test which results in a central deformation zone and a single pin-sized detached spall or perforation is considered minimally above the failure threshold (≥).

Of the 81 impact tests there were 50 pass results and 31 failures.

One key feature of metallic open-cell foams is their ability to induce multiple shocks in projectile and

bumper fragments through secondary impacts with individual foam ligaments. The non-isentropic shock and isentropic release process induces higher entropies (or internal energies), leading to projectile fragmentation, melting, and vaporization at lower impact velocities than for traditional shielding configurations (e.g. Whipple shield). The multi-shock shield, for example, was designed to utilize this phenomenon by distributing the weight of a single bumper plate over multiple bumpers of aluminum or glass ceramic fabric. Visual inspection of aluminum multi-shock shields identified molten and thick vapor deposits at an impact velocity of 6.3 km/s that were representative of those on an aluminum Whipple shield at 10 km/s [3]. Similar shock heating enhancements were also identified numerically in [4]. As the majority of the tests reported in Table 1 were performed at, or around, the failure limit of the panel, the state of the debris cloud material cannot be inferred from witness plate deposits. Furthermore, the majority of failed targets exhibited rear facesheet damage consisting of a small number of pin-sized perforation holes (generally one or two). For the high-speed tests these perforation holes were commonly at the apex of a bulged region, whereas the low speed tests rarely showed additional facesheet damage. It is reasonable to conclude, therefore, that although enhanced fragmentation, melting, and vaporization of projectile and front facesheet fragments is expected (compared to that for impact on a Whipple shield), failure was generally induced by the impact of individual solid projectile fragments, rather than an impulsive loading by a finely dispersed fragment cloud, even at high velocities.

Table 1. Summary of impact testing

Test no.	*Target*	d_p *(mm)*	θ *(deg)*	V *(km/s)*	*Result*
3147-3[+]	0.5" Al F10	1.2	0	6.83	>
3147-4[+]	0.5" Al F10	1.2	0	6.87	>
3147-1[+]	0.5" Al F10	1.0	0	6.95	<
3147-2[+]	0.5" Al F10	1.1	0	6.89	≤
3148-1[+]	0.5" Al F10	1.2	45	7.13	<
3148-2[+]	0.5" Al F10	1.3	45	6.9	<
5045-1[+]	0.5" Al F10	1.4	45	7.02	<
3148-3[+]	0.5" Al F10	1.3	60	6.97	<
3148-4[+]	0.5" Al F10	1.4	60	6.85	<
5045-2[+]	0.5" Al F10	1.5	60	6.91	<
5036-3[+]	0.5" Al F40	1.4	0	6.45	>
5036-1[+]	0.5" Al F40	1.0	0	6.88	<
5036-2[+]	0.5" Al F40	1.2	0	6.9	<
8589	0.5" Al F40	1.3	0	2.43	=
5037-2[+]	0.5" Al F40	1.4	45	6.92	=
5037-1[+]	0.5" Al F40	1.2	45	7.05	<
8571	0.5" Al F40	1.4	45	6.68	<
8572	0.5" Al F40	2.0	60	6.7	≥
8582	0.5" Al F40	2.5	60	2.63	≥
8580	0.5" Al F40	1.8	60	6.79	≤
8581	0.5" Al F40	2.0	60	2.28	<<
8261	1.0" Al F10	2.0	0	6.87	≥
8280	1.0" Al F10	2.1	0	2.18	>
8269	1.0" Al F10	2.7	45	7.04	>
8268	1.0" Al F10	2.5	45	6.62	<<
8272	1.0" Al F10	3.2	60	6.7	>
8252	1.0" Al F20	2.5	0	6.88	>
8253	1.0" Al F20	2.0	0	6.85	≥
8276	1.0" Al F20	2.1	0	2.46	>
8254	1.0" Al F20	1.9	0	6.87	<<
8425	1.0" Al F20	2.3	0	4.71	<
8255	1.0" Al F20	2.5	45	7.1	>
8257	1.0" Al F20	2.5	45	6.46	≥
8256	1.0" Al F20	2.3	45	6.88	<
8259	1.0" Al F20	3.2	60	7.1	≥
8258	1.0" Al F20	3.0	60	7.13	≤
8260	1.0" Al F20	3.2	60	6.68	<<
8263	1.0" Al F40	2.0	0	6.52	≥
8279	1.0" Al F40	3.4	0	2.62	>>
8422	1.0" Al F40	2.5	0	2.75	>
8424	1.0" Al F40	2.3	0	4.68	=
8423	1.0" Al F40	2.1	0	2.34	>
9320	1.0" Al F40	3.0	0	7	>>
9321	1.0" Al F40	2.7	0	6.94	=
9322	1.0" Al F40	2.8	0	6.59	≥
9323	1.0" Al F40	2.6	0	5.88	=
8567	1.0" Al F40	1.9	0	2.2	<<
8568	1.0" Al F40	2.0	0	6.63	<<
8585	1.0" Al F40	2.0	0	4.43	<<
9072	1.0" Al F40	2.2	0	3.11	<
9073	1.0" Al F40	2.2	0	5.36	<<
9074	1.0" Al F40	2.0	0	7.56	<<
8420	1.0" Al F40	2.5	45	2.44	=
8569	1.0" Al F40	2.7	45	6.66	>
8270	1.0" Al F40	2.5	45	6.78	<<
8271	1.0" Al F40	2.7	45	6.99	<
8421	1.0" Al F40	2.2	45	2.68	<
8427	1.0" Al F40	2.6	45	4.78	<<
8428	1.0" Al F40	2.8	45	4.76	<<
9075	1.0" Al F40	2.5	45	3.76	<<
8267	1.0" Al F40	3.2	60	6.57	<<
9007	1.0" Al F40	3.4	60	6.91	<
4161[+]	2.0" Al F10	4.0	0	6.89	≥
4151[+]	2.0" Al F10	3.6	0	6.76	<
4163[+]	2.0" Al F40	4.0	0	6.79	≥
4152[+]	2.0" Al F40	3.6	0	6.79	<
8590	2.0" Al F40	4.0	0	2.7	<
8573	2.0" Al F40	5.2	45	6.98	≥
4155[+]	2.0" Al F40	4.0	45	6.89	<
4156[+]	2.0" Al F40	4.0	45	6.84	<
4162[+]	2.0" Al F40	4.4	45	6.92	<
4164[+]	2.0" Al F40	4.4	45	6.7	<
5068[+]	2.0" Al F40	4.8	45	6.93	<
8613	2.0" Al F40	7.0	60	2.73	>
8591	2.0" Al F40	5.7	60	6.74	<
8614	2.0" Al F40	6.0	60	6.74	<
9220	2.0" Al F40	6.0	60	2.74	≤
9324	1.0” Al F40	3.0	0	6.71	>
9357	1.0” Al F40	2.4	0	3.25	<
9358	1.0” Al F40	2.5	0	5.48	>
9359	1.0” Al F40	2.3	0	7.38	>
9360	1.0” Al F40	2.8	45	3.52	>
9362	1.0” Al F40	2.9	45	5.50	<
9363	1.0” Al F40	2.5	45	7.19	≤
9374	1.0” Al F40	2.6	0	6.66	<
9376	1.0” Al F40	3.4	45	6.72	>

[+] Previously reported in [5]

3.1 Scatter assessment

Due to the non-homogeneity of the foam microstructure and the characteristic failure mechanism observed in the experiments, the issue of performance scatter may be more relevant for foam core sandwich panels than traditional shielding configurations. In order to assess the scatter, a series of six impact experiments were performed at nominally identical conditions (2.7 mm diameter projectile, 45° incidence, 6.8 km/s) on the 1.0" Al F40 target. A comparison of the core and rear wall damages of the six target specimens is made in Fig. 3. Of the six tests, one resulted in perforation (HITF08569) (d_h = 2.0 mm), while the other five showed various degrees of rear wall plastic deformation. Of the non-perforated targets, the damage cone generally extended through ~90% of the core thickness. The exception to this is HITF09067, which shows penetration through less than 80% of the core thickness.

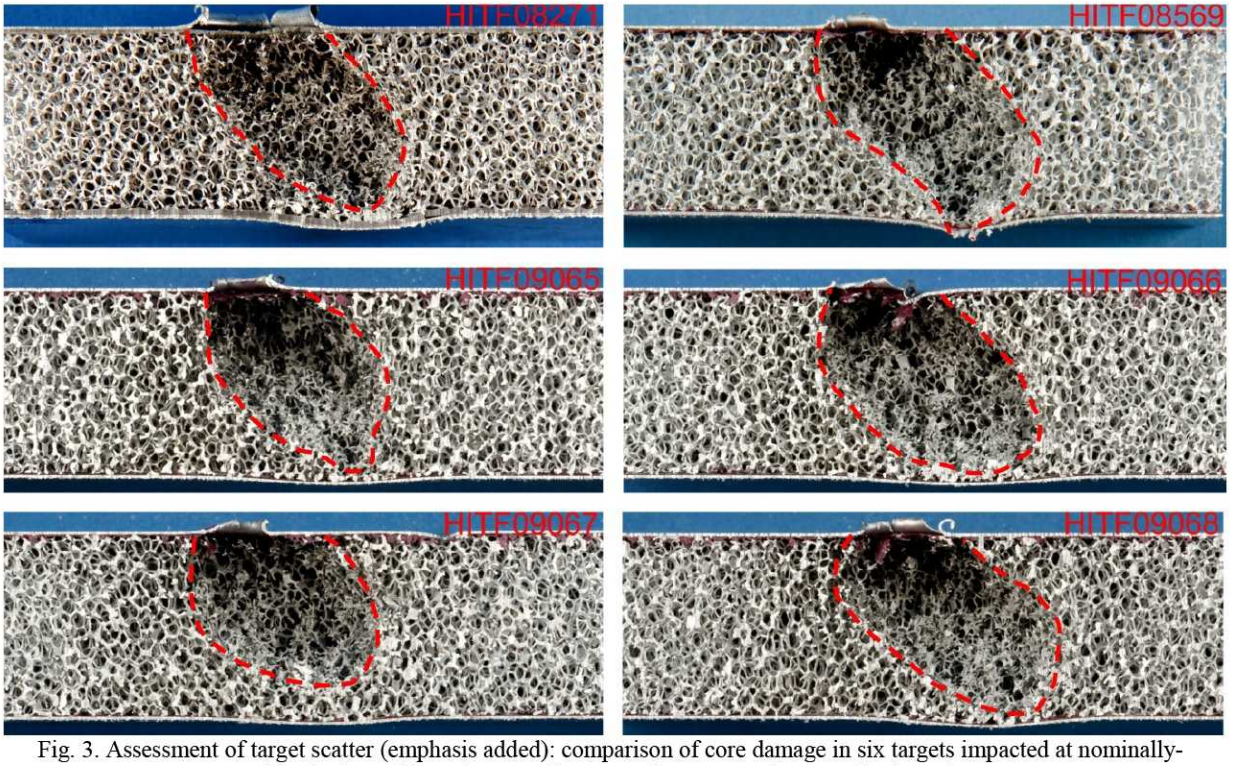

Fig. 3. Assessment of target scatter (emphasis added): comparison of core damage in six targets impacted at nominally-identical conditions (2.7 mm diameter Al2017-T4 sphere, 6.8 km/s, 45°)

4. The effect of pore density on shielding performance

In order to evaluate the effect of pore density on shielding performance three variations were considered in this study: 10, 20, and 40 PPI. A comparison of the three foam structures is shown in Fig. 4. The cell size, pore size, and ligament width of the three foams are provided in Table 2.

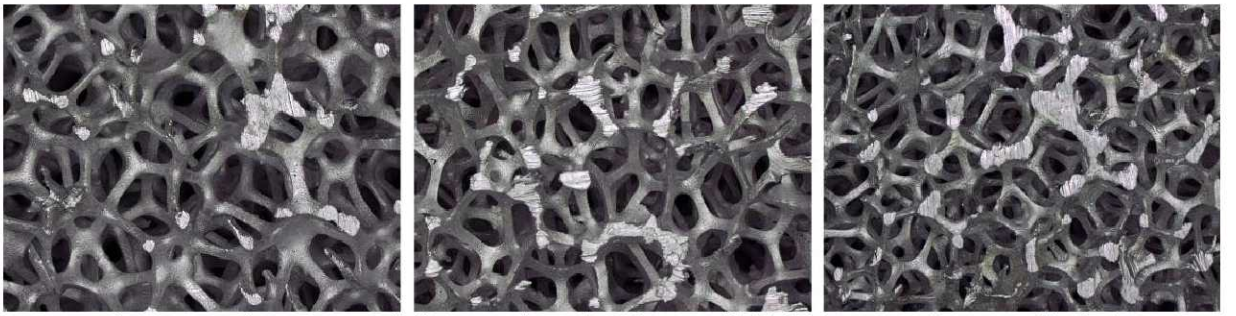

Fig. 4. Comparison of 10 PPI (left), 20 PPI (center), and 40 PPI (right) foam structure (×20 magnification)

Table 2. Characteristic measurements of the three foam cores.

Pore density	*Cell size (mm)*	*Pore size (mm)*	*Ligament width (μm)*
10 PPI	3.95	2.33	382
20 PPI	3.28	1.78	329
40 PPI	2.63	1.59	251

Pore density is expected to affect the shielding performance of metallic foam through a number of mechanisms, for example:

1. Higher pore densities should increase the number of secondary impacts of projectile and front facesheet fragments, providing increased shock heating than lower PPI cores
2. Increased pore density is expected to restrict gas expansion to a greater degree than lower PPI cores as a result of the smaller pores
3. Increased pore density is shown to decrease the width (or thickness) of foam ligaments, resulting in different fragment diameter to ligament thickness ratios for secondary impacts. This ratio can be compared to that of projectile diameter to bumper thickness, and as such, is expected to affect secondary shock heating and fragmentation.

A number of tests were performed at nominally identical conditions to investigate the effect of pore density on shielding performance, a summary of which is given in Table 3.

Table 3. Comparison of varying PPI shield performance at nominally-identical impact conditions.

Test no.	Nominal conditions			Result	Comments
[10/20/40 PPI]	θ (deg)	V (km/s)	d_p (mm)	[10/20/40 PPI]	
8280/8276/8423	0	2.5	2.1	> / > / >	All targets perforated with 1-2 small holes
8268/8257/8270	45	6.8	2.5	<< / ≥ / <<	No damage to 10 and 40 PPI target rear facesheets, single pin-sized perforation of 20 PPI panel
8261/8253/8263	0	6.8	2.0	≥ / ≥ / ≥	All targets with single small perforation hole
8272/8260/8267	60	6.8	3.2	> / << / <<	Small bulge on 20 and 40 PPI panel rear facesheets, single hole perforation of 10 PPI panel
3147-4/-/5036-2	0	6.8	1.2	> / - / <	Clear perforation of 10 PPI panel, 40 PPI no damage
3148-1/-/5037-1	45	6.8	1.2	< / - / <	No damage to rear facesheet of 10 and 40 PPI panels
5045-1/-/8571	45	6.8	1.4	< / - / <	Small bulge on 40 PPI panel rear facesheet, no damage to 10 PPI panel rear facesheet
4151/-/4152	0	6.8	3.57	< / - / <	No damage to rear facesheet of 10 and 40 PPI panels
4161/-/4163	0	6.8	4.0	≥ / - / ≥	Two small perforation holes in 10 PPI panel rear facesheet, single small perforation of 40 PPI panel

Although sensitive to scatter considerations, the shielding performance was found to improve with increasing pore density. To highlight this, a comparison of damages in 10, 20 and 40 PPI panels nominally impacted by a 2.0 mm diameter Al2017-T4 sphere at 6.8 km/s with normal incidence is shown in Fig. 5. In this figure, the 10 PPI panel is clearly perforated while the 20 and 40 PPI panels show only a slight bulge on the rear facesheet. Inspection of the sectioned cores shows that the extension of damage in the 20 PPI panel is deeper than in the 40 PPI panel, progressing through to the rear facesheet. In general, the higher pore density panels seem to be less susceptible to individual solid fragments passing through the core with few or no secondary impacts, leading to perforation cases like that of the 10 PPI panel in Fig. 5. The higher pore density cores also show an increased degree of densification, i.e. collapse of the foam cells, at the limits of the damage cone, suggesting a greater level of energy partitioning through plastic work (although the effect of this on penetration limits is expected to be minimal).

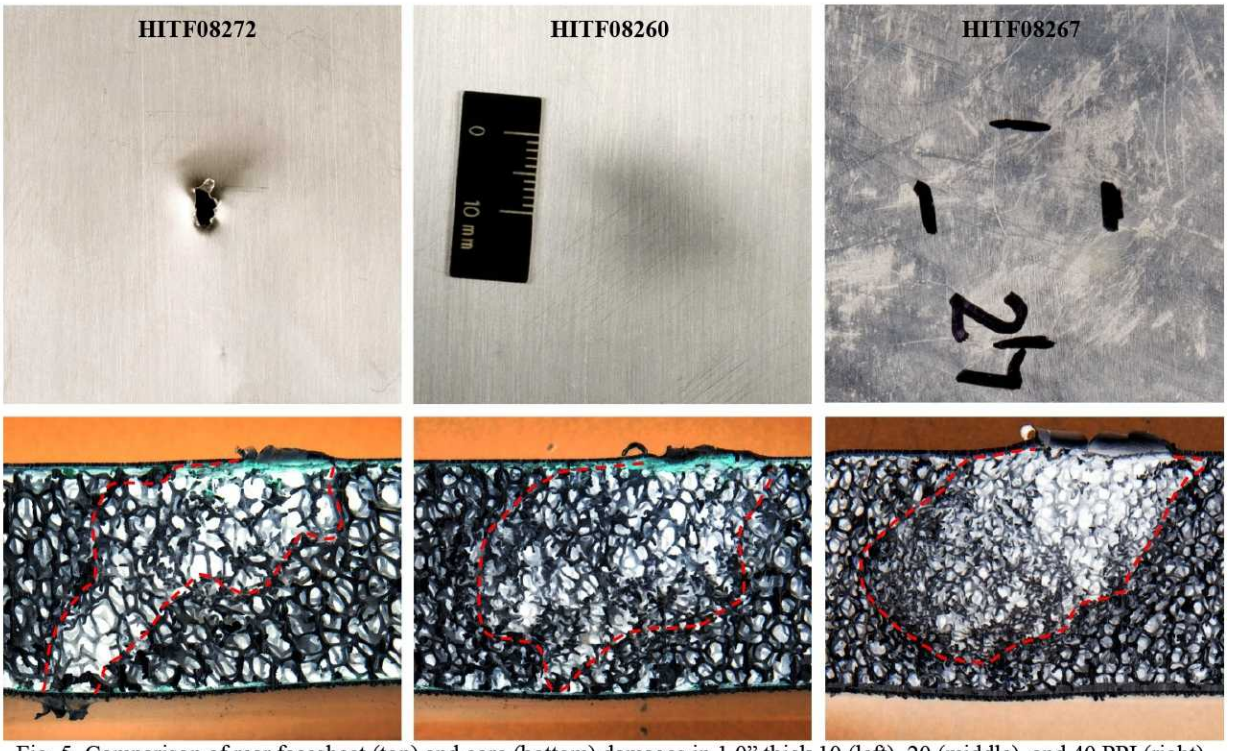

Fig. 5. Comparison of rear facesheet (top) and core (bottom) damages in 1.0" thick 10 (left), 20 (middle), and 40 PPI (right) foam core sandwich panels impacted by 3.2 mm Al2017-T4 diameter spheres at 6.65 ± 0.08 km/s and 60°. Color inversion applied to core images for visualization.

5. A ballistic limit equation for foam core sandwich panels

Penetration into porous media such as concrete, silica, and foams is generally described by a cratering relationship (e.g. [7]). However, clear evidence of increased performance with increasing velocity between 2.2 and 5.0 km/s was observed in the experiments – suggesting that the shielding behavior is similar to that of a spaced multi-wall shield. As such, a ballistic limit equation (BLE) based on the JSC Whipple shield equation [8] is derived. The JSC Whipple shield BLE is defined in three parts: a low velocity regime related to failure induced by an intact (albeit deformed) projectile; an intermediate velocity regime related to a partially fragmented (and possibly molten) projectile and bumper fragment cloud, and; a hypervelocity regime relating to a finely dispersed, predominantly

molten debris cloud which induces impulsive failure of the rear wall (rather than the cratering and spallation mechanism seen in the low- and intermediate velocity regimes). For the foam core sandwich panel, evidence of decreasing penetration depth with increasing projectile velocity is apparent at speeds below 3 km/s (e.g. HITF09072 vs HITF08423). As such, the low-to-shatter regime velocity limit, V_{LV}, is defined as:

$$V_{LV} = 2.25 \Big/ (\cos\theta)^{1/3}$$

In the low velocity regime, i.e. $V < V_{LV}$, the ballistic limit of an open-cell foam core sandwich panel is calculated as:

$$d_c = \frac{1.83\left(t_b + t_w(\sigma/40)^{0.5} + t_f^{1.1}(\rho_f/\rho_w)\right)}{\left(\rho_p^{0.5} \cdot V^{2/3} \cdot (\cos\theta)^{4/5}\right)^{18/19}} \tag{2}$$

where t_b is the front facesheet thickness (cm), t_w is the rear facesheet thickness (cm), σ is the rear facesheet yield strength (ksi), t_f is the foam core thickness (cm), ρ_f is the volumetric density of the foam core (g/cm^3), ρ_w is the rear facesheet material density (g/cm^3), ρ_p is the projectile material density (g/cm^3), V is velocity (km/s), θ is the impact angle measured normal to the target surface (deg), and d_c is the critical projectile diameter. Eq. (2) includes the foam core in the maximum allowable penetration depth via determination of an equivalent aluminum plate thickness based on near linear density scaling. Additionally, angle dependence is increased to $(cos\ \theta)^{4/5}$ from the Whipple shield relationship, indicating a more substantial performance enhancement with increasing obliquity.

Secondary impacts of projectile and bumper fragments on individual foam ligaments have been found to increase the thermal state of penetrating particles, leading to fragmentation, melt, and vaporization at lower impact velocities than traditional shields. However, in this study, impulsive failure of the rear

wall was not observed in any of the impact experiments. Rather, the failure threshold was defined by the perforation of individual solid (or molten) fragments across the investigated range of impact velocities. Given the non-homogeneity of the foam structure on a micro scale, it is conceivable that individual fragments are able to penetrate the depth of the core with significantly fewer secondary impacts on foam ligaments. Subsequently, not only are the foam core panels subject to a greater degree of experimental scatter than traditional shields, the definition of the hypervelocity impact regime must be reconsidered. For this particular shielding configuration, the transition from shatter to hypervelocity regime (V_{HV}) is considered to occur once an increase in projectile velocity results in increased penetration depth and, hence, rear facesheet damage, defined as:

$$V_{HV} = 4.0 \Big/ \left(\cos\theta\right)^{1/3}$$

In the hypervelocity regime the foam core sandwich panel ballistic limit equation is defined as:

$$d_c = 1.915 \frac{\left(t_w + 0.5\, AD_f / \rho_w\right)^{2/3} t_f^{\,0.45} \left(\sigma/70\right)^{1/3}}{\rho_p^{\,1/3} \rho_b^{\,1/9} V^{2/5} \cos\theta^{4/5}} \tag{4}$$

where AD_f is the foam core areal density (g/cm^2) and ρ_b is the density of the front facesheet material. The effect of the foam core is included through an increase in the rear wall thickness corresponding to 50% of an equivalent areal weight plate, and an increase in core thickness (or facesheet spacing, S) dependence from 1/3 to 0.45. Kinetic energy scaling is used for extrapolation of the Whipple shield BLE to hypervelocities. Although considered a conservative approach, limitations of experimental facilities prevent verification or adoption of proposed surrogate validation techniques (e.g. cadmium scaling, numerical simulation, etc.). However, as transition to hypervelocity is considered to occur much earlier for the foam sandwich panel shield, a less conservative extrapolation is made in Eq. (4), i.e. $V^{2/3} \rightarrow V^{2/5}$. Additional modifications are made to the angle dependence and scaling constant of

the baseline Whipple equation.

In the intermediate regime, i.e. $V_{LV} < V < V_{HV}$, linear interpolation is applied:

$$d_c = d_c\left(V_{LV}\right) + \frac{\left(d_c\left(V_{HV}\right) - d_c\left(V_{LV}\right)\right)}{V_{HV} - V_{LV}} \times \left(V - V_{LV}\right) \tag{5}$$

The ballistic limit equation is derived for application with 40 PPI foam core panels. As described previously, the performance of the 40 PPI foams was found to be superior to that of the 20 and 10 PPI panels, however the variation was generally minimal and often difficult to differentiate from experimental scatter. For application with the 10 and 20 PPI panels, a 5% decrease in the predicted critical projectile diameter in the hypervelocity regime should be applied.

In Fig. 8 through Fig. 10 the ballistic limit equation is expressed as a curve, demarcating between impact conditions expected to lead to failure of the structural panel, and those against which the shield is capable of defending. Test data is also included in the figures. Of the 86 impact tests reported in Table 1, 62 (72%) are predicted accurately, nineteen tests (22.1%) are slightly conservatively predicted (i.e. $d_p/d_c < 1.2$), one (1.2%) is conservatively predicted ($d_p/d_c < 1.5$) and four (4.7%) are non-conservatively predicted. However, the four non-conservative predict a critical projectile diameter of within 1.5% of the test value (i.e. $d_p/d_c > 98.5\%$), which is considered well within the experimental scatter bounds. In Fig. 11 the predictions of the BLE are plotted in terms of d_p/d_c ratio for all the test data reported in Table 1.

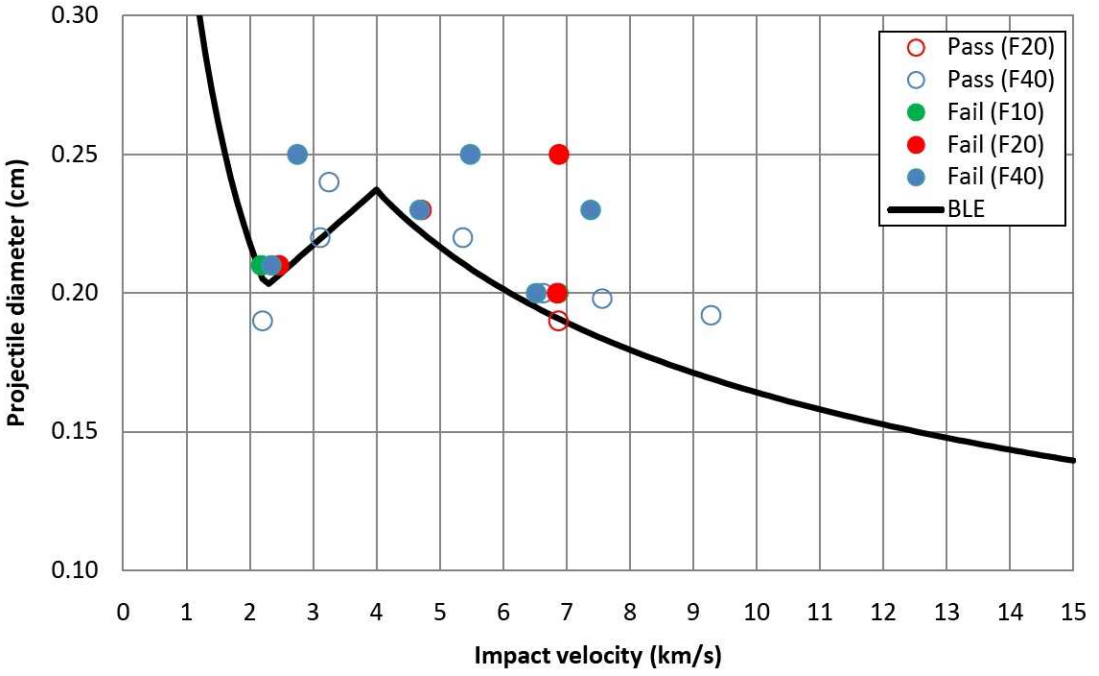

Fig. 6. Ballistic limit curve for the 1.0" Al foam sandwich panel at normal incidence.

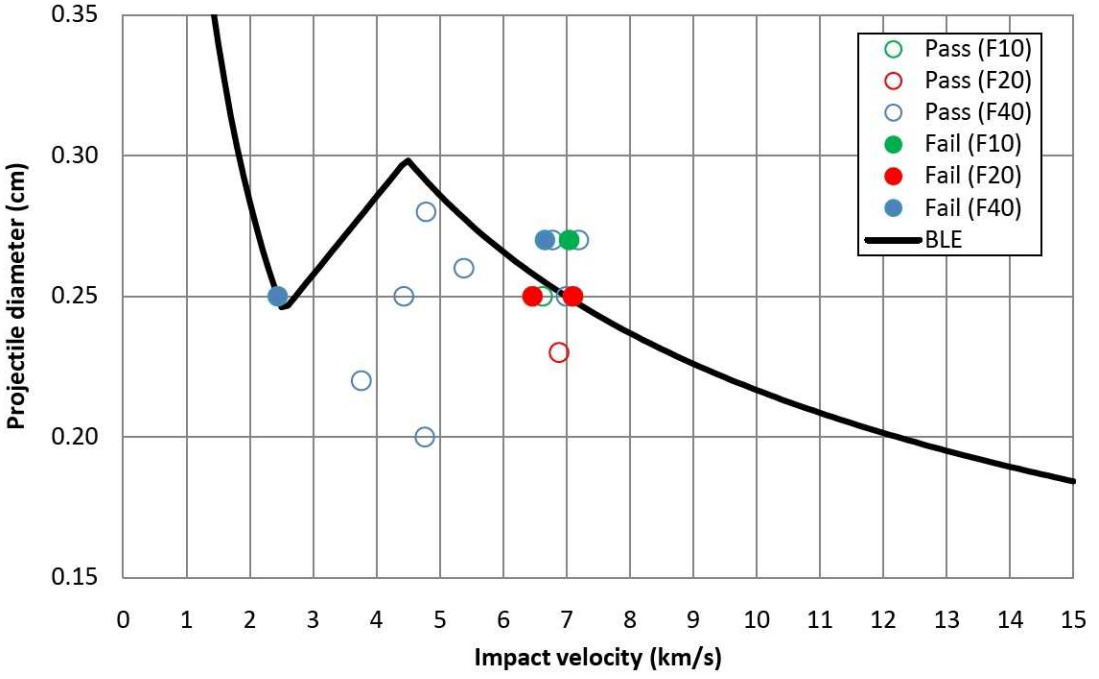

Fig. 7. Ballistic limit curve for the 1.0" Al foam sandwich panel at 45°.

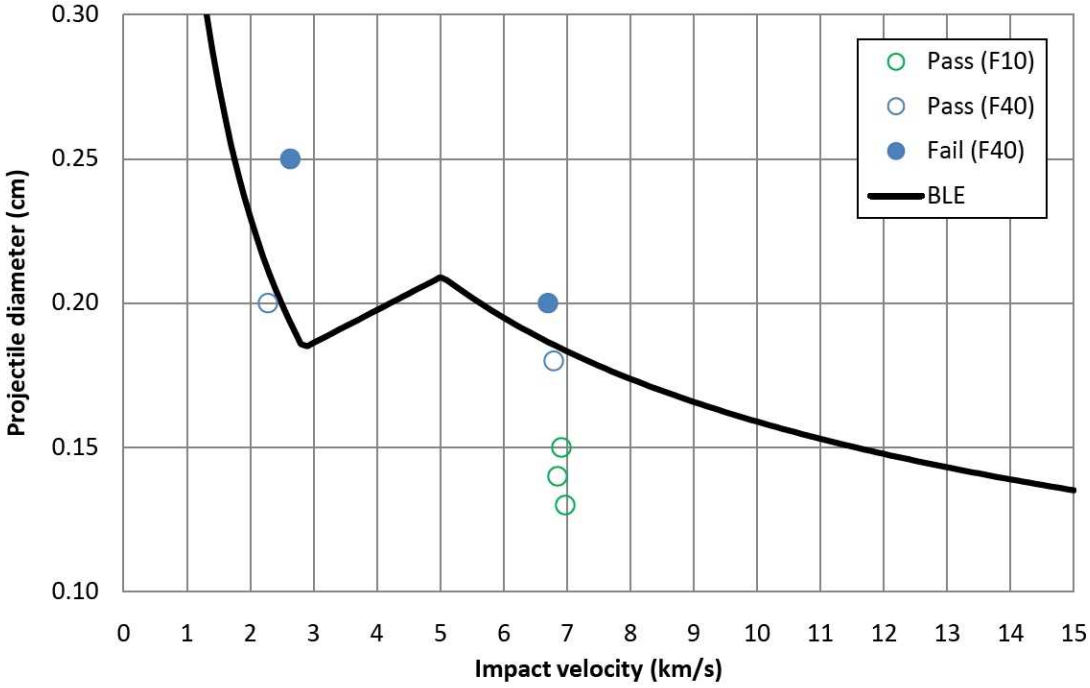

Fig. 8. Ballistic limit curve for the 0.5" Al foam sandwich panel at 60°.

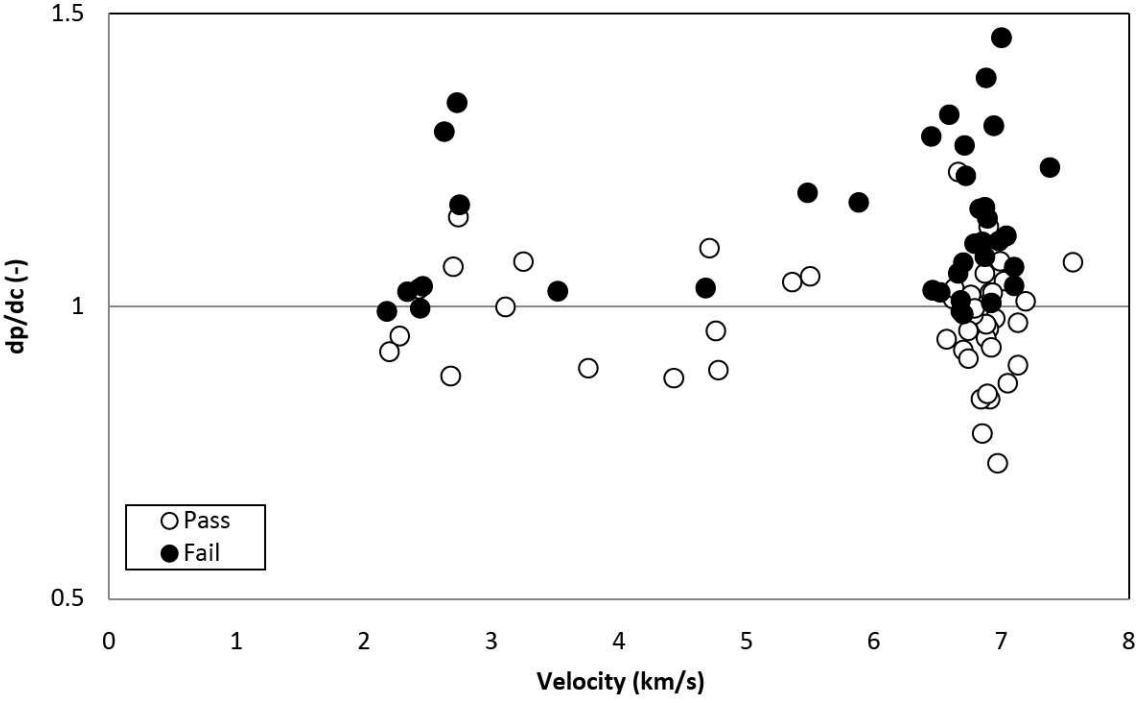

Fig. 9. Summary of the test results and BLE predictions.

6. Comparison to traditional shielding configurations

In order to evaluate the shielding performance of the foam core sandwich panels, the derived ballistic limit equation can be compared to those of other common shield types. In Fig. 9 the foam BLE is plotted against flight-representative examples of a metallic Whipple shield [8], stuffed Whipple shield [9], and honeycomb sandwich panel [10]. It should be noted that the Whipple shield and stuffed Whipple shield curves have been de-rated according to additional non-ballistic mass required for installation of non-structural shielding components. For the Whipple shield, 30% of the bumper mass is approximated for non-ballistic requirements [9], while 35% of the total shield mass is deducted for the stuffed Whipple configuration [11]. The foam sandwich panel is shown to perform superior to the other configurations at low velocities (<5 km/s), yet poorer than the Whipple and stuffed Whipple shields at hypervelocity (although still highly superior to the honeycomb sandwich panel).

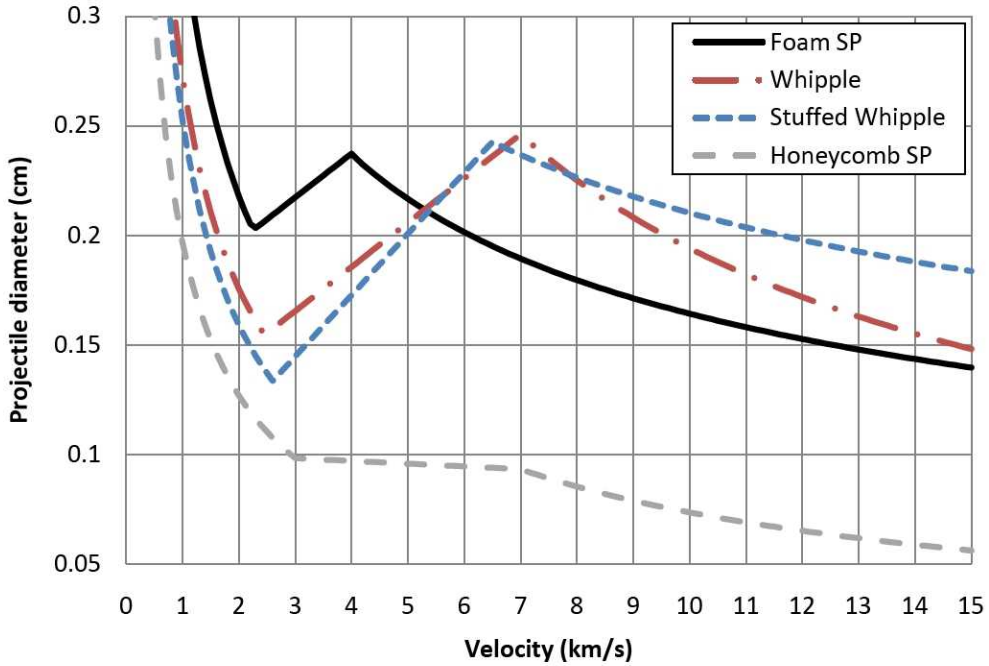

Fig. 10. Comparison of ballistic limit curves for comparable weight/standoff MMOD shield types.

At orbital altitudes common for manned spaceflight (i.e. ~400 km), a general rule of thumb is that the median velocity for MMOD risk is approximately 7 km/s. For these missions, the performance of the foam sandwich panel evaluated in this study is expected to provide similar protection levels to the Whipple and stuffed Whipple configurations considered in Fig. 9. However, for missions dominated by higher velocity debris (e.g. interplanetary), mission risk will clearly be lower for traditional Whipple-based configurations.

7. Summary and Conclusions

Metallic open cell foams are of interest for micrometeoroid/debris shielding as they provide comparable mechanical and thermal performance to traditional structures such as honeycomb sandwich panels without MMOD-shielding detrimental though-thickness channeling cells. Preliminary investigations have demonstrated the potential of these structures in complex configurations (e.g. double layer foam bumpers [12]), however, to date there has not been a comprehensive study to characterize the performance of standalone foam core sandwich panels and the effect of design variables such as pore size, relative density, core thickness, and facesheet thickness on their shielding capability. In this study a total of 86 hypervelocity impact tests were performed on aluminum open cell foam core sandwich panel structures, with varying impact conditions (velocity, angle, projectile diameter) and target configurations (facesheet thickness, core thickness, pore density). From the test results, shielding performance was found to increase (albeit minimally) with increasing pore density. Furthermore, secondary impacts of projectile and front facesheet fragments on individual foam ligaments was considered to result in fragmentation, melt, and vaporization at lower velocities than for traditional shielding configurations due to increased thermal energy from the non-isentropic shock and

isentropic release processes. A ballistic limit equation, based on the JSC Whipple shield BLE was derived for the foam core structures, for use in risk assessment tools such as BUMPER. The equation was shown to accurately predict 72% of the test results, with the remaining 25% conservatively predicted (four non-conservative predictions were within 1.5% of the failure limit, considered to be well within the experimental scatter bounds). The low-shatter, and shatter-hypervelocity regime limits of the BLE were defined at 2.25 km/s and 4.0 km/s respectively, reflecting the enhanced thermal heating induced by impact on the foam structure.

The performance of the foam core sandwich panels was compared against that of traditional MMOD shields, taking into account installation requirements for non-structural configurations (i.e. non-ballistic mass). The foam panel was shown to perform significantly better than honeycomb core sandwich panels over the range of velocities considered (0-15 km/s), demonstrating the substantial protection enhancement possible for vehicles without a dedicated protective structure. The performance of the foam panel was superior to that of the scaled Whipple and stuffed Whipple shields at velocities below 5 km/s, however the traditional shields were superior at higher velocities. For large vehicles, or missions operating in highly polluted orbits (e.g. 800-1000 km altitude) the stuffed Whipple shield remains the most desirable protective configuration. However, for unmanned missions, or vehicles with extreme weight or volume restrictions, the open cell foam core sandwich panel structure represents a feasible new alternative. Furthermore, it is considered that optimization of these structures may lead to sizeable improvements in protective capability and efficiency.

Acknowledgements

All testing was performed at the NASA JSC White Sand's Test Facility in Las Cruces, NM.

References

[1] Sennett R, Lathrop B. Effects of hypervelocity impact on honeycomb structures. *Journal of Spacecraft*, 1968; **5**(12): 1496-1497.

[2] Schonberg W. Characterizing ejecta from oblique high speed impacts. *8th International Symposium on Ballistics*, San Antonio, 1999: p. 1176-1183.

[3] Cour-Palais B, Crews J. A multi-shock concept for spacecraft shielding, *International Journal of Impact Engineering* 1990; **10**: 135-146.

[4] Alme M, Christiansen E, Cour-Palais B. Hydrocode simulations of the multi-shock meteoroid and debris shield, *Shock Compression of Condensed Matter* 1991, American Physical Society, p. 975-978.

[5] Yasensky J, Christiansen E. Hypervelocity impact evaluation of metal foam core sandwich structures, NASA Johnson Space Center, Houston, 2008, NASA/TP-2008-214776.

[6] Chu C, Chen Y, Hseu G, Hwang D. The study of obliquity on the ballistic performance of basket fabric composite materials, *Journal of Composite Materials* 2007; **41**(13): 1539-1558.

[7] Cour-Palais B. Hypervelocity impact investigations and meteoroid shielding experience related to Apollo and Skylab, *Orbital Debris* 1985: 247-275.

[8] Christiansen E. Design and performance equations for advanced meteoroid and debris shields, *International Journal of Impact Engineering* 1993; **14**: 145-156.

[9] Christiansen E. Meteoroid/Debris Shielding, NASA Johnson Space Center, Houston, 2003, TP-2003-210788

[10] Ryan S, Christiansen E. Micrometeoroid and orbital debris (MMOD) shield ballistic limit analysis program, NASA Johnson Space Center, Houston, 2009, NASA/TM-2009-214789.

[11] Destefanis R, Schaefer F, Lambert M, Faraud M, Schneider E. Enhanced space debris shields for manned spacecraft, *International Journal of Impact Engineering* 2003; **29**: 215-226.

[12] Ryan S, Hedman T, Christiansen E. Honeycomb vs. foam: evaluating a potential upgrade to International Space Station module shielding for micrometeoroids and orbital debris, NASA Johnson Space Center, Houston, 2009, NASA/TM-2009-214793.